The Astrophysical Journal, 634:1202–1213, 2005 December 1


# MERGERS OF NEUTRON STAR–BLACK HOLE BINARIES WITH SMALL MASS RATIOS: NUCLEOSYNTHESIS, GAMMA-RAY BURSTS, AND ELECTROMAGNETIC TRANSIENTS

S. Rosswog
School of Engineering and Science, International University Bremen, Campus Ring 1, Bremen 28759, Germany
*Received 2005 February 19; accepted 2005 August 5*

## ABSTRACT

We discuss simulations of the coalescence of black hole–neutron star binary systems with black hole masses between 14 and 20 $M_\odot$. The calculations use a three-dimensional smoothed particle hydrodynamics code, a temperature-dependent, nuclear equation of state, and a multiflavor neutrino scheme. General relativistic effects are mimicked using the Paczyński-Wiita pseudo-potential and gravitational radiation reaction forces. Unlike previous, purely Newtonian calculations, in none of the explored cases does episodic mass transfer occur. The neutron star is always completely disrupted after most of its mass has been transferred directly into the hole. For black hole masses between 14 and 16 $M_\odot$ an accretion disk forms; large parts of it, however, are inside the last stable orbit and therefore falling with large radial velocities into the hole. These disks are (opposite to the neutron star merger case) thin and—except for a spiral shock—essentially cold. For higher mass black holes ($M_{\rm BH} \geq 18\ M_\odot$) almost the entire neutron star disappears in the hole without forming an accretion disk. In these cases the surviving material is spun up by tidal torques and ejected as a half-ring of neutron-rich matter. None of the investigated systems is a promising gamma-ray burst (GRB) central engine. We find between 0.01 and 0.2 $M_\odot$ of the neutron star to be dynamically ejected. Like in a Type Ia supernova, the radioactive decay of this material powers a light curve with a peak luminosity of a few times $10^{44}$ ergs s$^{-1}$. The maximum is reached about 3 days after the coalescence and is mainly visible in the optical/near-infrared band. The coalescence itself may produce a precursor pulse with a thermal spectrum of $\sim$10 ms duration.

*Subject headings:* black hole physics — gamma rays: bursts — hydrodynamics — methods: numerical — nuclear reactions, nucleosynthesis, abundances

*Online material:* color figures

## 1. INTRODUCTION

Neutron star binary systems were already recognized as potential central engines of GRBs two decades ago: they were mentioned in Paczyński (1986) and Goodman et al. (1986) and discussed in more detail by Eichler et al. (1989; for a more complete bibliography we refer to existing reviews, e.g., Mészáros 2002; Piran 2005). As a variant of the neutron star binary case, Paczyński (1991) discussed systems containing a neutron star (NS) and a stellar mass black hole (BH) as a possible GRB engine. These days, such compact binary systems are considered the standard model for the subclass of short GRBs, which typically last for about 0.3 s (Kouveliotou et al. 1993). Most recently, on 2005 May 9, the first ever X-ray afterglow for a short ($\sim$30 ms), hard GRB (GRB 050509b) was detected (Bloom et al. 2005). Its tentative association with a nearby giant elliptical galaxy has been interpreted as indicating a compact binary merger origin of this burst (Bloom et al. 2005; Lee et al. 2005a). While NS-BH binaries are usually just considered to be a minor variation of a double neutron star merger (DNS), it has been pointed out recently (Rosswog et al. 2004) that this is not obvious and that such a coalescence automatically produces a hot and massive accretion disk around the hole. Therefore, its role for GRBs requires further investigation.

During the disruption process tidal torques are expected to eject material into highly eccentric, possibly unbound orbits. This debris is extremely neutron-rich, $Y_e \sim 0.1$, and therefore (if ejected at appropriate rates) holds the promise to be one of the still much debated sources of *r*-process elements (Lattimer & Schramm 1974, 1976). Moreover, NS-BH systems are generally considered to be promising sources for ground-based gravitational wave detectors such as the Laser Interferometer Gravitational-Wave Observatory (LIGO; Abramovici et al. 1992), GEO600 (Wiilke et al. 2003), VIRGO (Caron et al. 1997), and TAMA (Tagoshi et al. 2001).

It is worth pointing out in this context that there is a controversy about the rates at which NS-BH mergers occur. Bethe & Brown (1998) argued that NS-BHs should merge about an order of magnitude more frequently than DNSs, while a recent study by Pfahl et al. (2005) concludes that the number of NS-BH systems in the Galaxy should be below 1% of the number of double neutron star systems. To date eight DNSs have been observed (Stairs 2004), while not a single NS-BH binary has yet been discovered.

Neutron star–black hole merger simulations have been performed by several groups. Most of the simulations use Newtonian or pseudo-Newtonian gravity. Janka et al. (1999) used a grid-based hydrodynamics code together with a nuclear equation of state (EOS) and a neutrino leakage scheme to explore the role of these mergers in a GRB context. Lee (2000, 2001) and Lee & Kluzniak (1999a, 1999b) used smoothed particle hydrodynamics with polytropic EOSs to explore the sensitivity of the results to the adiabatic exponent of the EOS. Lee & Ramirez-Ruiz (2002) have analyzed the flow pattern within an accretion disk around a BH, and in recent papers (Lee et al. 2004, 2005b) they included detailed microphysics in their simulations. Setiawan et al. (2004) constructed disks around stellar mass black holes and followed their evolution, including explicit viscosity, while Rosswog et al. (2004) investigated the dynamics of the accretion process.

Recently, there has been progress in the relativistic treatment of black hole–neutron star binaries. Taniguchi et al. (2005), for example, have constructed quasi-equilibrium black hole–neutron star binaries in general relativity, and further efforts with approximate relativistic treatments seem to be underway (Rasio et al. 2005).

Stellar mass black holes formed in core collapse supernovae are thought to be born with masses ranging from about 3 to 20 $M_\odot$ (Fryer & Kalogera 2001). Numerical simulations have so far only explored black hole masses up to 14 $M_\odot$ (Janka et al. [1999], Lee & Kluzniak [1999a, 1999b], and Lee [2000, 2001] used black holes up to 10 $M_\odot$; Rosswog et al. [2004] explored masses up to 14 $M_\odot$). In this paper we focus on black holes with masses ranging from 14 to 20 $M_\odot$. The 14 $M_\odot$ case has been explored previously (Rosswog et al. 2004) using the same microphysics but a purely Newtonian BH potential and may therefore serve to gauge the effect of the Paczyński-Wiita pseudo-potential.

A simple estimate for the radius where a star around a BH is disrupted is the tidal radius, $R_{\rm tid} = (M_{\rm BH}/M_{\rm NS})^{1/3} R_{\rm NS}$. As this scales more slowly with the black hole mass ($\propto M_{\rm BH}^{1/3}$) than the gravitational radius ($\propto M_{\rm BH}$), it is expected that higher mass BHs will have more difficulties building up massive disks. Therefore, the lower end of the black hole mass distribution is most promising for the launch of a GRB. Unfortunately, it is very difficult to find suitable approximations for these cases, as here the spacetime is far from a static Schwarzschild/Kerr solution, and therefore neither the use of pseudo-potentials nor solving the hydrodynamics equations in a fixed background metric are admissible. For these cases fully dynamical general relativistic calculations are needed.

In this paper we explore the accretion dynamics and the observational signatures of the high-mass end of these binary systems.

## 2. SIMULATIONS

We use a three-dimensional smoothed particle hydrodynamics code that has been developed to simulate compact objects. Most of the code features have been described elsewhere (Rosswog et al. 2000, 2003; Rosswog & Davies 2002; Rosswog & Liebendörfer 2003) and are only briefly mentioned here for the sake of completeness. For the simulations described here we have changed to an integration scheme with individual time steps; also, the treatment of the black hole is different from previous implementations.

In our implementation we have taken particular care to avoid artifacts from the use of artificial viscosity. The quantities $\alpha$ and $\beta$ that are usually used as fixed parameters in the artificial viscosity tensor (Gingold & Monaghan 1983) are made time dependent and evolved by solving an additional differential equation (Morris & Monaghan 1997). In the absence of shocks $\alpha = \alpha^* = 0.1$ [we always use $\beta(t) = 2\alpha(t)$], to be compared with the standard values of $\alpha = 1$ and $\beta = 2$. In strong shocks our $\alpha$ is allowed to rise up to values of 2 in order to avoid postshock oscillations (Rosswog et al. 2000). In addition, the Balsara (1995) prescription is used to avoid spurious forces in pure shear flows. Thus, artificial viscosity is essentially absent unless a shock is detected. These measures have proved very effective, suppressing unwanted effects of artificial viscosity by orders of magnitude (Rosswog et al. 2000; Rosswog & Davies 2002).

We use a temperature-dependent nuclear equation of state that is based on the tables provided by Shen et al. (1998a, 1998b) and that has been smoothly extended to the low-density regime (Rosswog & Davies 2002). It covers a density range in $\log(\rho)$ from 0.5 to 15.4, temperatures from 0 to 100 MeV, and electron fractions $Y_e$ from 0 to 0.5. The nucleons are treated in the framework of temperature-dependent relativistic mean field theory. At densities below about $\frac{1}{3}$ of nuclear matter density, nuclei are present in the plasma. Its composition is determined for fixed $\rho$, $T$, and $Y_e$ from an equilibrium of nucleons, alpha particles, and an average heavy nucleus. Thus, energy release due to nuclear transmutations is accounted for in a simple way. Contributions of photons and electrons/positrons of an arbitrary degree of relativity and degeneracy are added to the thermodynamic quantities. Details can be found in Rosswog & Davies (2002).

Nowhere (except in the initial neutron stars) is $\beta$-equilibrium assumed. Local changes in the electron fraction and the thermal energy content of matter due to neutrinos are accounted for with a multiflavor neutrino treatment (Rosswog & Liebendörfer 2003).

The Newtonian self-gravity of the neutron star fluid is calculated using a binary tree (e.g., Benz et al. 1990). This makes the star less compact and might—at least quantitatively—influence the accretion process. We use a Paczyński-Wiita potential to approximately take into account the presence of general relativistic effects around the black hole, such as the presence of a last stable orbit. Clearly, the use of the Paczyński-Wiita potential is not a complete substitute for fully fledged general relativistic hydrodynamic simulations around a Schwarzschild black hole. It has, however, turned out to be astonishingly accurate: test-particle orbits with $r < 6\,M_{\rm BH}$ (geometrical units with $G = c = 1$ are used throughout the paper) are unstable, and orbits with $r < 4\,M_{\rm BH}$ are unbound; i.e., the radius of the marginally stable orbit is located at $R_{\rm isco} = 6\,M_{\rm BH}$, and the radius of the marginally bound orbit is $R_{\rm mb} = 4\,M_{\rm BH}$. Direct comparisons with general relativistic solutions in a Schwarzschild spacetime show that the pseudo-potential is able to capture the essentials of general relativity and can reproduce accretion disk structures to an accuracy of better than 10% (see, e.g., Artemova et al. 1996). The pseudo-potential does not, however, prevent velocities from becoming larger than unity. Abramowicz et al. (1996) suggested a rescaling of the velocities found using Newtonian models together with the Paczyński-Wiita potential (i.e., in our case the numerical velocities: $v_{\rm num} = v_{\rm phys}\tilde{\gamma}$, where $\tilde{\gamma} = [1 - (v_{\rm phys})^2]^{-1/2}$). They found this rescaling to reproduce the exact relativistic velocities to better than 5%. This could be used, for example, to calculate Doppler shifts; this rescaling is not, however, used in this paper.

The buildup of the binary tree from scratch is computationally expensive; therefore, we do not remove the particles that have crossed our inner boundary (located at $R_{\rm bd} = 3\,M_{\rm BH}$) at each time step. They are only removed when a dump is written, i.e., every $2.5 \times 10^{-5}$ s, which is as short as 1/12 of the neutron star dynamical timescale and therefore does not lead to any artifacts (this has been confirmed by removing particles at every time step). To avoid numerical problems with the singularity of the Paczyński-Wiita potential we have extended it smoothly with a polynomial (see the Appendix and Fig. 11). Note that all particles that have ever encountered a deviation from the Paczyński-Wiita potential inside $R_{\rm bd}$ are removed at the next dump.

We have implemented two different time-integration schemes with individual time steps: a second-order Runge-Kutta-Fehlberg method (Fehlberg 1968) and a second-order predictor-corrector scheme. Both of these schemes have been tested extensively against a Runge-Kutta-Fehlberg scheme with a global time step. As the results were nearly indistinguishable, the simulations were run with the predictor-corrector method, as it only requires one force evaluation per time step. The most time-consuming part of

these simulations is the inspiral where (due to the stiff neutron star EOS and the resulting flat stellar density profile) practically all particles have to be evolved on the shortest time step. The gain in speed for the presented calculations is moderate (factors of a few), but in other test problems the code was faster by more than 2 orders of magnitude.

We construct our initial neutron stars by solving the Lane-Emden equations for our EOS with the additional constraint of (cold) $\beta$-equilibrium. This yields stellar radii of about 16 km for a 1.4 $M_\odot$ neutron star. All smoothed particle hydrodynamics (SPH) particles have the same mass, to avoid numerical noise arising from interactions of particles with unequal masses. Prior to setting up the binary system the neutron stars are relaxed carefully by applying additional, velocity-proportional damping forces in the equations of motion so that the SPH particles can settle into their equilibrium positions. Once such an equilibrium is obtained the NS-BH binary system is set up, with either a tidally locked or a nonspinning neutron star. The locked systems are constructed accurately using the hydrocode itself (see Rosswog et al. 2004). The nonspinning neutron stars are set on orbit with an angular frequency determined by the force balance between centrifugal and gravitational forces. In all cases the radial velocity component of a point-mass binary of the considered separation is added.

The simulations presented here use up to $3\times10^6$ SPH particles and are currently the best resolved models of neutron star black hole encounters (Rosswog et al. [2004] used up to $10^6$ particles; Lee [2001] used slightly more than 80,000 particles).

## 3. RESULTS

### 3.1. *Merger Dynamics*

The dynamics of the coalescence is illustrated in Figures 1 and 2.[1] In all of the cases the neutron star is completely disrupted after a large portion of its mass has been transferred directly into the hole. The corresponding peak accretion rates exceed 1000 $M_\odot\,\mathrm{s}^{-1}$ for about 1 ms; after this short episode they drop by at least 2 orders of magnitude (see Fig. 3, *left*).

It is instructive to compare the 14 $M_\odot$ case to the corresponding case of our previous study (Rosswog et al. 2004), in which we used a Newtonian BH potential. In the purely Newtonian case we found episodic mass transfer with a low-mass "mini–neutron star" surviving throughout the whole simulation, or about eight close encounters. In the Paczyński-Wiita case about 1.15 $M_\odot$ (see Fig. 3, *right*) are transferred directly into the hole; the rest forms a rapidly expanding tidal tail. The tidal tail still contains an outward-moving density maximum (corresponding to the mini–neutron star of the Newtonian case), but its self-gravity is not strong enough to form a spherical object. The results are well converged: runs 1 and 2 show excellent agreement in the BH masses and peak mass transfer rates. Some minor deviations are visible at low mass transfer rates (see Fig. 3, *left*, and the distance, $R_{\mathrm{MT}}$, where numerically resolvable mass transfer sets in; see col. [7] in Table 1).

The case with 16 $M_\odot$ BHs behaves qualitatively very similar to that of 14 $M_\odot$ BHs: slightly more mass (about 1.2 $M_\odot$) is transferred into the hole, and the disk is slightly less massive, hot, and dense than that in the 14 $M_\odot$ case. Again, the two different resolutions yield nearly identical results.

The systems containing BHs of 18 $M_\odot$ or more (runs 5, 6, and 9) do not form accretion disks at all. Almost the entire neutron star flows via the inner Lagrange point directly into the hole; only a small fraction of the star is spun up enough by tidal torques to be dynamically ejected (see col. [6] of Table 2). In these cases the remnant consists of the black hole (without any accretion disk) and a rapidly expanding, concentric (half-)ring of neutron-rich debris material (0.08 $M_\odot$ for the 18 $M_\odot$ BH, and 0.01 $M_\odot$ for the 20 $M_\odot$ BH; see Fig. 2). The result—that it seems to be intrinsically difficult to form promising accretion disks (at least for the investigated mass ratios)—is consistent with recent estimates of Miller (2005).

### 3.2. *Disk Structure*

A hot and thick accretion disk around a black hole is believed to be an essential ingredient for a GRB. As described in § 3.1, and as expected from simple analytical estimates, more promising disks form for larger mass ratios, i.e., smaller BH masses. In the described simulations only systems with BH masses below 18 $M_\odot$ form an accretion disk at all. Here the most promising case, run 2 ($M_{\mathrm{BH}} = 14\,M_\odot$; tidal locking), is discussed; the $q = 0.1$ case with a nonrotating neutron star (run 7) looks very similar.

In those cases where a disk forms, substantial parts of it are inside the innermost stable circular orbit at $R_{\mathrm{isco}} = 6\,M_{\mathrm{BH}}$ and are therefore "plunging" with large radial velocities toward the hole, which leads to a substantial consumption of the disks during the simulated time. For illustration, Figure 4 shows the distribution of the SPH particles at $t = 18.396$ ms of run 2. Also shown are the projections of the particles onto the orbital ($XY$) plane (*black*), and overlaid are the projections to the $XZ$ plane of those particles $j$ with $|y_j| < 150$ km (*gray*), in order to show the vertical disk structure. The loci of the Schwarzschild radius and $R_{\mathrm{isco}}$ are also shown. While the matter cross section far away from the hole is close to circular, the disk close to the hole is geometrically thin [$|z| \ll \bar{\omega} = (x^2 + y^2)^{1/2}$], except for the region close to the spiral shock where the accretion stream interacts with itself. In this region the disk is slightly puffed up. Due to the plunge motion, only moderate densities [$\log(\rho) < 10.5\ \mathrm{g\,cm}^{-3}$] and temperatures are reached (see Fig. 5). The disk is essentially cold, except for the spiral shock, where the temperatures reach $\sim$2.5 MeV.

The geometrically *thin*, relatively cool disks that we find for black hole masses between 14 and 16 $M_\odot$ are in stark contrast to the *thick* disks that form in the neutron star merger case (see Figs. 15 and 16 in Rosswog & Davies 2002).

### 3.3. *Neutrino Emission*

The annihilation of neutrino-antineutrino pairs is one way for energy to be deposited in the baryon-free region above the hole. In cases with black hole masses $\geq$18 $M_\odot$, the neutrino emission is negligible ($<10^{46}$ ergs $\mathrm{s}^{-1}$). The most promising cases are, as expected, the ones with the lowest black hole masses. If disks form at all, they are completely transparent to the emerging neutrinos. In lowest mass cases, with $M_{\mathrm{BH}} = 14\,M_\odot$ (runs 1, 2, and 7), we find peak luminosities of $L_{\nu,\mathrm{tot}} = L_{\nu_e} + L_{\bar{\nu}_e} + L_{\nu_x} \approx 10^{51}$ ergs $\mathrm{s}^{-1}$ (where the index $x$ refers to the heavy lepton neutrinos); i.e., our most promising cases here yield luminosities that are more than 2 orders of magnitude smaller than those in our neutron star merger calculations where the same microphysics was used. The average energies of the emitted neutrinos are between 12 and 15 MeV. Unlike the neutron star merger case, the neutrino luminosity does not settle into a stationary state, since the disk is being consumed on a timescale of tens of ms. In the tidally locked case we find a single neutrino pulse of about 20 ms

[1] Movies can be found at http://www.faculty.iu-bremen.de/srosswog/movies.html.

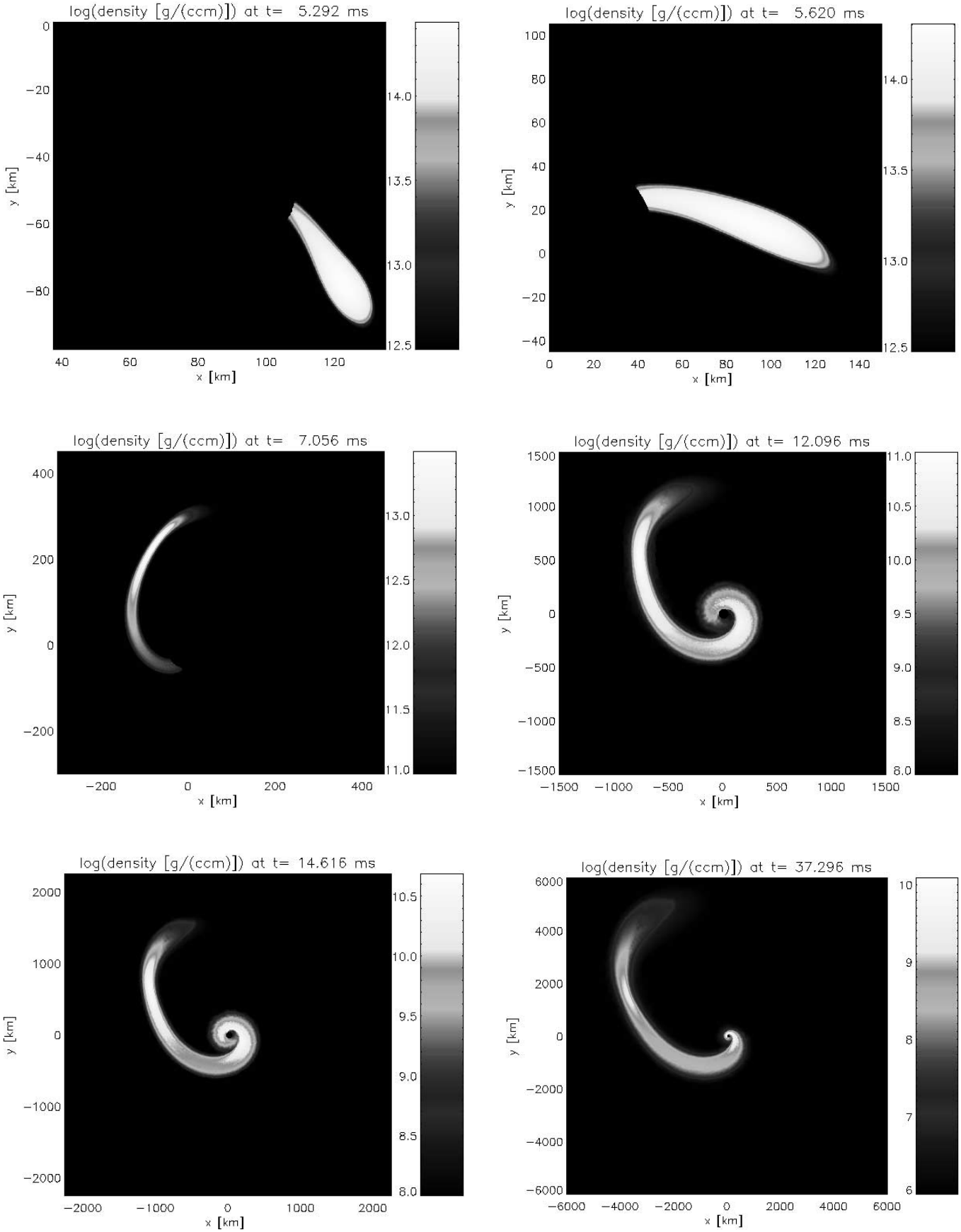


FIG. 1.—Density in the orbital plane of run 2 ($q = 0.1$; tidally locked neutron star). [*See the electronic edition of the Journal for a color version of this figure.*]

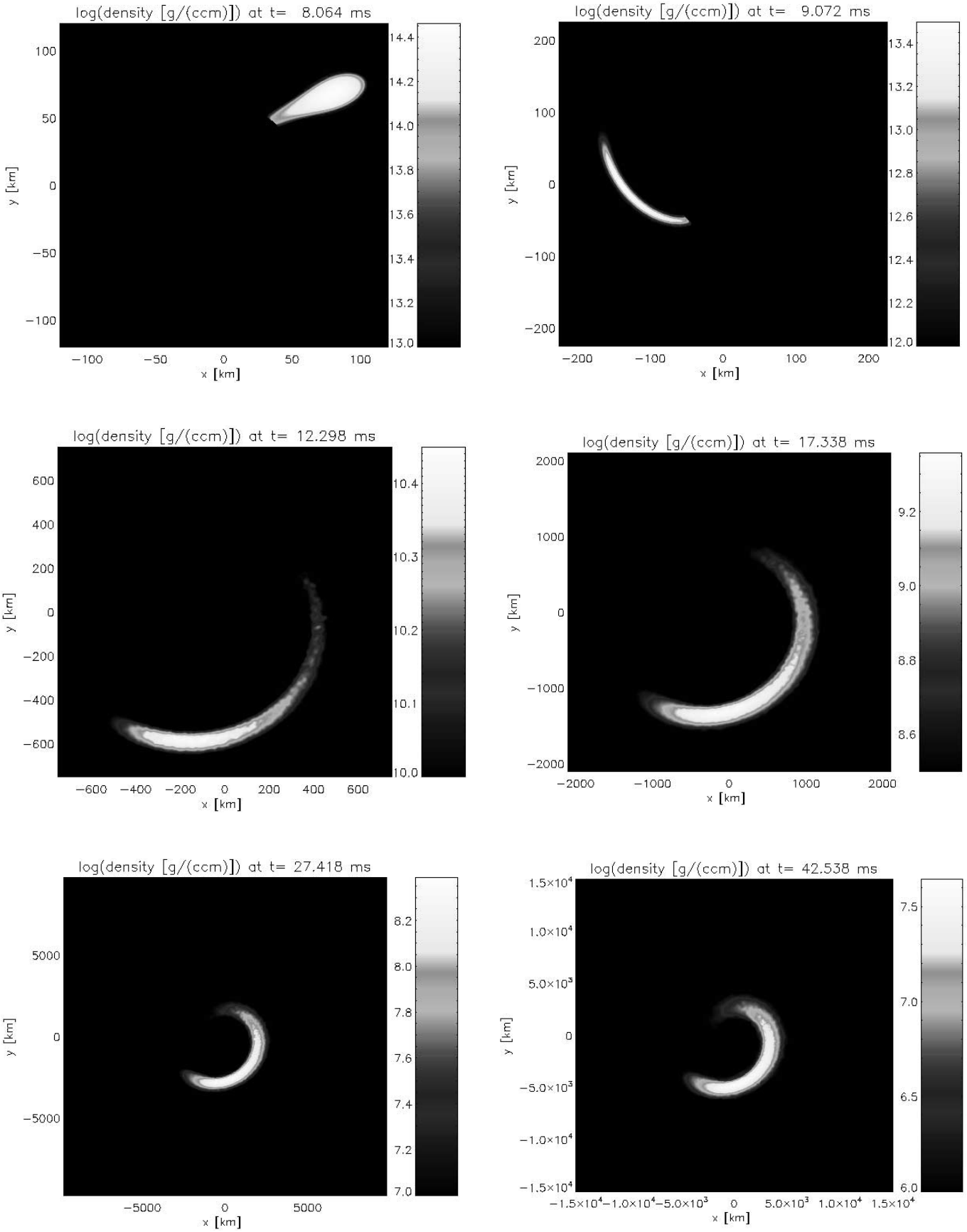


FIG. 2.—Density in the orbital plane of run 5 ($q = 0.0778$; tidally locked neutron star). [*See the electronic edition of the Journal for a color version of this figure.*]

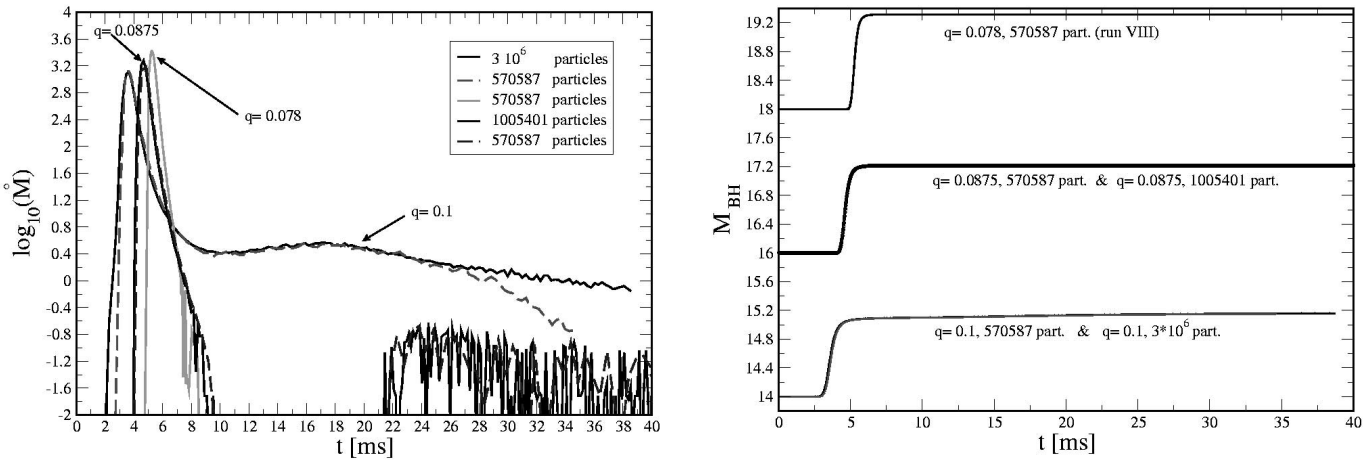


FIG. 3.—*Left*: The mass transfer rates as a function of time. In one case ($q = 0.078$; i.e., $M_{\rm BH} = 18\ M_\odot$) the mass transfer stops completely. This is also true for the $20\ M_\odot$ case (not shown). *Right*: The growth of the black hole with time is shown for five of the runs. Note that the runs that simulate the same systems (runs 1 and 2; runs 3 and 4) with different resolutions yield nearly identical curves. [*See the electronic edition of the Journal for a color version of this figure*.]

TABLE 1

SUMMARY OF THE DIFFERENT RUNS

| Run (1) | $M_{\rm BH}/q$ (2) | NS Spin (3) | $R_{\rm tid}$ (4) | $a_0$ (5) | $R_{\rm isco}$ (km) (6) | $R_{\rm MT}$ (km) (7) | Particle No. (8) | $T_{\rm sim}$ (ms) (9) |
|---|---|---|---|---|---|---|---|---|
| 1..... | 14/0.1 | C | 36.1 | 127.5 | 124.1 | 117 | 570587 | 34.6 |
| 2..... | 14/0.1 | C | 36.1 | 127.5 | 124.1 | 125 | 2971627 | 40.8 |
| 3..... | 16/0.0875 | C | 37.7 | 145.5 | 141.8 | 122 | 570587 | 78.1 |
| 4..... | 16/0.0875 | C | 37.7 | 145.5 | 141.8 | 123 | 1005401 | 60.9 |
| 5..... | 18/0.0778 | C | 39.3 | 162.0 | 159.6 | 123 | 570587 | 50.4 |
| 6..... | 20/0.07 | C | 40.7 | 187.5 | 177.3 | 128 | 1503419 | 179.6 |
| 7..... | 14/0.1 | I | 36.1 | 126.2 | 124.1 | 116 | 1497453 | 49.8 |
| 8..... | 16/0.0875 | I | 37.7 | 143.9 | 141.8 | 121 | 1497453 | 39.8 |
| 9..... | 18/0.0778 | I | 39.3 | 160.4 | 159.6 | 126 | 1497453 | 205.4 |

NOTES.—Col. (1): Run. Col. (2): $M_{\rm BH}$: black hole mass in solar units; $q = M_{\rm NS}/M_{\rm BH}$. Col. (3): NS spin: C = tidally locked; I = nonspinning neutron star. Col. (4): $R_{\rm tid}$: tidal radius. Col. (5): $a_0$: initial separation. Col. (6): $R_{\rm isco}$: last stable orbit Schwarzschild black hole. Col. (7): $R_{\rm MT}$: distance where numerically resolvable mass transfer sets in. Col. (8): Particle no.: SPH particle number. Col. (9): $T_{\rm sim}$: simulated duration.

TABLE 2

RESULTS OF THE DIFFERENT RUNS

| Run (1) | $M_{\rm BH}/q$ (2) | $a_{\rm BH}$ (3) | $L^{\rm peak}_{\nu,{\rm tot}}$ (ergs s$^{-1}$) (4) | $M_{\rm ej}$ (5) | $E_{\rm kin,ej}$ (ergs) (6) |
|---|---|---|---|---|---|
| 1..... | 14/0.1 | 0.196 | $8 \times 10^{50}$ | 0.20 | $2.7 \times 10^{52}$ |
| 2..... | 14/0.1 | 0.200 | $8 \times 10^{50}$ | 0.20 | $2.8 \times 10^{52}$ |
| 3..... | 16/0.0875 | 0.197 | $3 \times 10^{50}$ | 0.15 | $2.1 \times 10^{52}$ |
| 4..... | 16/0.0875 | 0.197 | $2 \times 10^{50}$ | 0.15 | $2.1 \times 10^{52}$ |
| 5..... | 18/0.0778 | 0.201 | $<10^{46}$ | 0.08 | $1.3 \times 10^{52}$ |
| 6..... | 20/0.07 | 0.198 | $<10^{46}$ | 0.01 | $2.2 \times 10^{51}$ |
| 7..... | 14/0.1 | 0.203 | $1 \times 10^{51}$ | 0.17 | $2.2 \times 10^{52}$ |
| 8..... | 16/0.0875 | 0.206 | $6 \times 10^{49}$ | 0.11 | $1.3 \times 10^{52}$ |
| 9..... | 18/0.0778 | 0.207 | $<10^{46}$ | 0.04 | $5.6 \times 10^{51}$ |

NOTES.—Col. (1): Run. Col. (2): $M_{\rm BH}$: black hole mass in solar units; $q = M_{\rm NS}/M_{\rm BH}$. Col. (3): $a_{\rm BH} = J_{\rm BH}/M^2_{\rm BH}$ is the dimensionless black hole spin parameter at the end of the simulation ($J_{\rm BH}$ is the angular momentum transferred into the hole). Col. (4): $L^{\rm peak}_{\nu,{\rm tot}}$ is the peak luminosity of the sum of all neutrino flavors. Col. (5): $M_{\rm ej}$ refers to the material (in solar masses) that is dynamically ejected during the merger. Col. (6): $E_{\rm kin,ej}$: kinetic energy in ejecta at end of simulation.

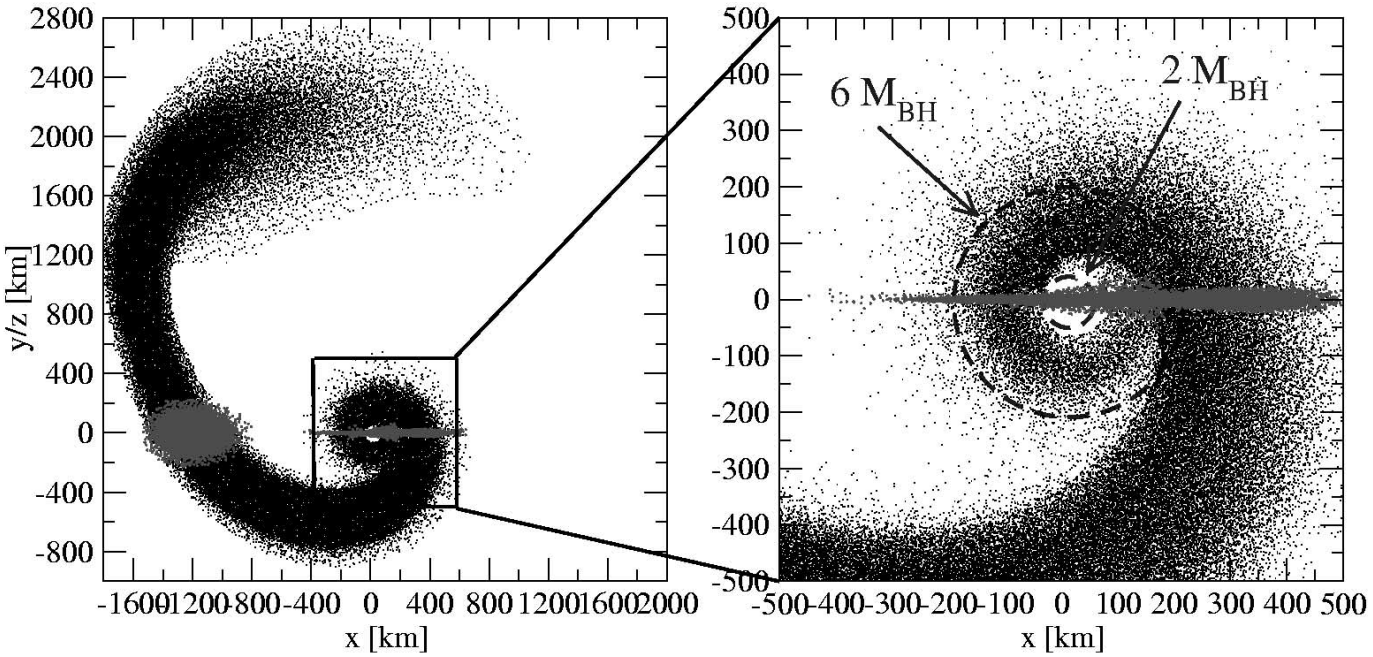


FIG. 4.—Projections of the SPH particle positions onto the orbital plane (run 2 at $t = 18.396$ ms). Overlaid are the projections to the *XZ* plane of those particles with $|y_i| < 150$ km, the positions of the Schwarzschild radius, and the innermost stable circular orbit of a test particle around a Schwarzschild black hole. In regions of high column number densities, only a fraction of the particles are displayed. [*See the electronic edition of the Journal for a color version of this figure*.]

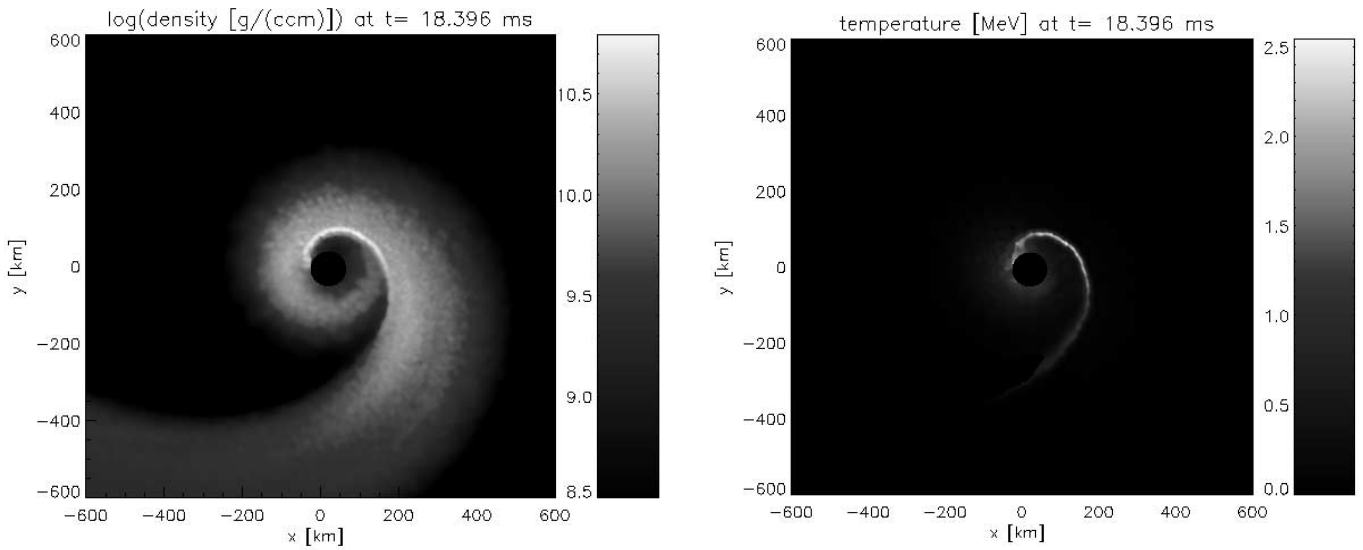


FIG. 5.—Blow-up of the inner disk region of run 2 at $t = 18.396$ ms after simulation start [*left panel*: log (density); *right panel*: temperature]. Clearly visible is the shock, where the accretion stream interacts with itself. [*See the electronic edition of the Journal for a color version of this figure*.]

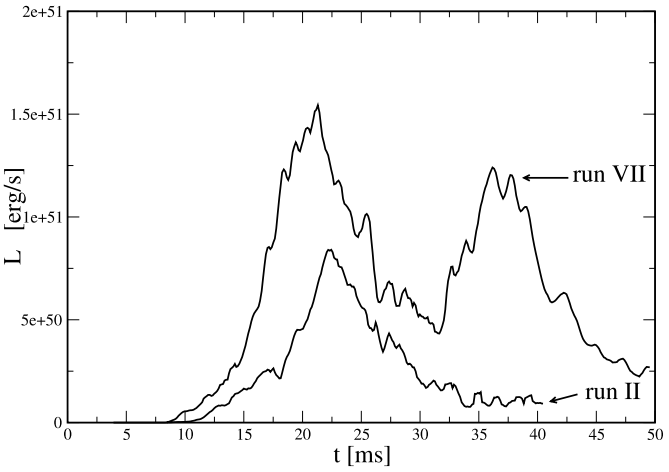


FIG. 6.—Total neutrino luminosities of runs 2 ($q = 0.1$; tidal locking) and 7 ($q = 0.1$; no neutron star spin).

duration; in the case without neutron star spin we find two neutrino pulses separated by about 15 ms (see Fig. 6).

## 4. SUMMARY AND DISCUSSION

We have performed three-dimensional hydrodynamic simulations of neutron black hole encounters with mass ratios $q = M_{\rm NS}/M_{\rm BH} \leq 0.1$. We used a state-of-the-art temperature-dependent, nuclear EOS; a detailed, multispecies neutrino treatment; and the Paczyński-Wiita pseudo-potential.

We consider all the approximations made to be valid to a high degree. If an accretion disk forms at all (i.e., for BH masses $<18\ M_\odot$) it is of only moderate density ($\sim 10^{10}$ g cm$^{-3}$) and completely transparent to neutrinos. Therefore, the neutrino emission results cannot be influenced by the flux-limited diffusion treatment. Moreover, the results are numerically converged: different numerical resolutions yield almost identical results. The BHs are massive enough to dominate the spacetime completely, and as they are spun up to spin parameters of only 0.2 (see Table 2), we consider the use of Paczyński-Wiita (PW) potentials a very good approximation (note that for $a = 0.2$ the event horizon moves from 2 to 1.98, and the last stable orbit moves from 6 to 5.33 gravitational radii; see Fig. 7).

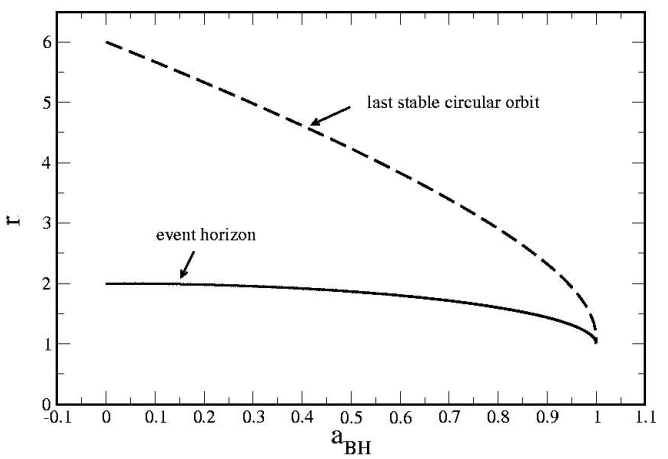


FIG. 7.—Position of the event horizon and the last stable circular orbit around a spinning black hole (see Novikov & Frolov 1989) as a function of the spin parameter $a_{\rm BH} = J_{\rm BH}/M_{\rm BH}^2$.

### 4.1. *Implications for Nucleosynthesis*

The ejected mass fraction found in these simulations is generally *very* large (see Table 2) but comparable to the analytical estimates of Lattimer & Schramm (1974, 1976), who estimated $0.05 \pm 0.05\ M_\odot$. We previously performed previously nucleosynthetic calculations for the decompressed ejecta in the neutron star merger case (Freiburghaus et al. 1999). As these calculations did not account for $Y_e$-changes due to weak interactions, $Y_e$ was treated as a free parameter and was varied in a range that is reasonable for neutron star material (0.05 to 0.20). For values between 0.08 and 0.15 we found an almost perfect agreement with the observed, solar system *r*-process abundances from around barium up to beyond the platinum peak. The value of $Y_e$ has basically two effects: (1) it determines the neutron to seed ratio and thus the maximum nucleon number $A$ of the resulting abundance distribution, and (2) the location of the reactions in the *N*-*Z* plane, the so-called *r*-process path, which is, in this case, very close to the neutron drip line. This path determines the nuclei that are involved and therefore the nuclear energy release and the corresponding $\beta$-decay timescales. The initial neutron star material is decompressed via the expansion and therefore continuously changes its composition. Starting from very large initial nuclei with hundreds of nucleons (the details of which are determined by the distributions of density, temperature, and electron fraction) these transmutations release nuclear binding energy until a final, $\beta$-stable composition has been reached. Figure 8 shows the snapshot distribution of $Y_e$ within the debris of run 2 at $t = 18.396$ ms; in Figure 9 $Y_e$ has been binned with the ejecta mass for the NS-BH cases with $q = 0.1$. Generally, as the only parts that have ever reached high temperatures disappear very quickly into the hole (see Fig. 5), the $Y_e$ of the ejected material closely reflects its initial value inside the neutron star. The values of $Y_e$ found are generally very close to what was found in the neutron star merger case to give excellent results (compare Freiburghaus et al. [1999] and Fig. 4; note, however, that due to the somewhat different expansion velocities, the interesting $Y_e$ values may be slightly different in the NS-BH case). To determine the exact elemental yields from these mergers is beyond the scope of the current work and is left to future investigations.

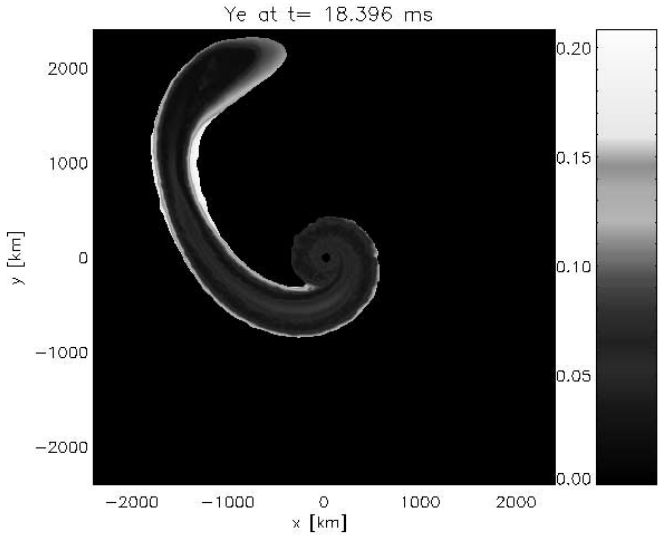


FIG. 8.—Electron fraction, $Y_e$, in the orbital plane (run 2; $q = 0.1$; tidal locking). The high-$Y_e$ skin around the remnant is the initial neutron star crust. [*See the electronic edition of the Journal for a color version of this figure.*]

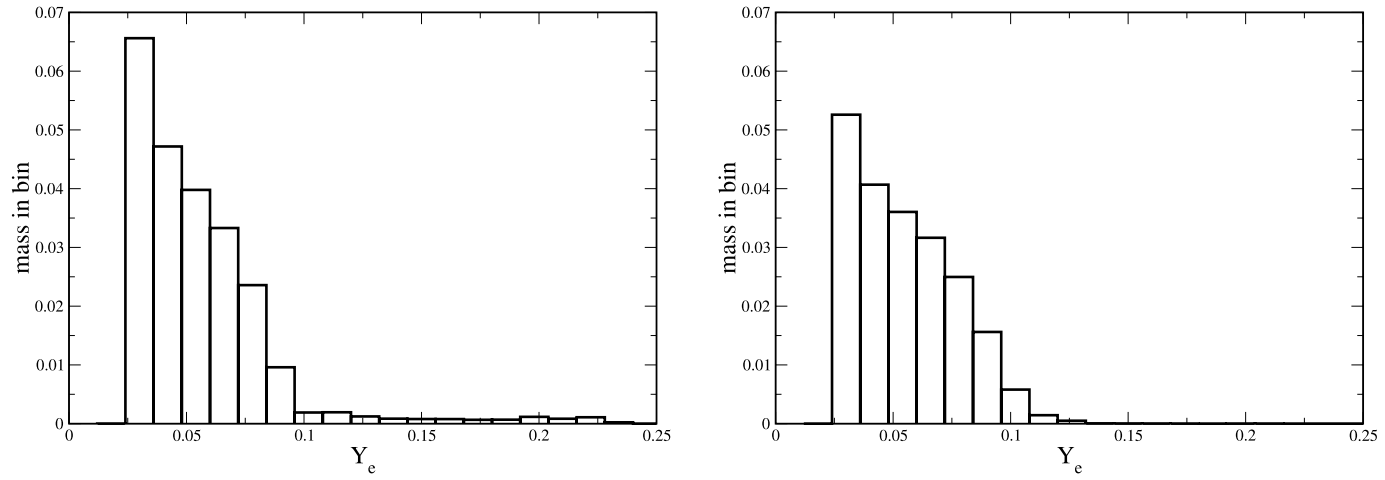


FIG. 9.—Histogram of the ejected mass binned according to $Y_e$. *Left*: Run 2 ($q = 0.1$; tidal locking). *Right*: Run 7 ($q = 0.1$; no neutron star spin). The missing high-$Y_e$ tail in the right panel may be an effect of the somewhat lower numerical resolution.

For the neutron star merger case, Argast et al. (2004) found that a conflict with the observed element ratios in metal-poor halo stars may arise if neutron star mergers were the *dominant* *r*-process source. Similar questions may be raised for the NS-BH case. One potential solution to the problem could be that NS-BHs coalesce much less frequently than DNSs. This would be consistent with the nonobservation of any NS-BH system (currently eight DNS systems are known; see Stairs 2004) and with results of recent studies (Pfahl et al. 2005) that estimate the NS-BH number in the Galactic disk to be less than 0.1%–1% of the number of DNSs.

We want to point out, however, that the ejecta found in our simulations exhibit very large radial velocities of $\approx 0.5c$. As most neutron star–black hole binaries are expected to merge in the outskirts of galaxies (see, e.g., Perna & Belczynski 2002), the chances are large that these high-velocity ejecta do not end up within the host galaxies, but rather enrich the intergalactic medium with very heavy, probably high-mass *r*-process elements. This interesting issue definitely requires further consideration in the future.

### 4.2. *Gamma-Ray Bursts*

The formation of a massive accretion disk around a black hole is thought to be a vital ingredient for a GRB central engine. None of the systems investigated in this study yields disks that are promising GRB engines. As the tidal radius only grows $\propto M_{\rm BH}^{1/3}$ while the gravitational radius of the BH scales $\propto M_{\rm BH}$, low-mass black holes would more easily form promising disks. In the simulations presented here, disks only form for BHs with masses below 18 $M_\odot$. As mentioned previously, these disks are essentially cold, except for a spiral shock with temperatures of $\approx$2.5 MeV. Unlike the neutron star merger case, these disks are geometrically *thin*, of only moderate density, and completely transparent to neutrinos. The peak densities in the shock are $\log(\rho) \approx 10.5$ cgs and lower elsewhere (see Fig. 5). This is to be compared with peak values of $\log(\rho) \approx 12$ cgs and $T \approx 4$ MeV in the neutron star merger case (Rosswog & Davies 2002). Moreover, the disk is drained substantially on the simulation timescale of a few tens of ms.

In the most promising cases the peak luminosities are about $10^{51}$ ergs s$^{-1}$ (see Table 2; Fig. 6). This is more than 2 orders of magnitude below the typical neutron star merger case (Rosswog & Liebendörfer 2003). The hot debris of a double neutron star coalescence deposits $\sim 10^{48}$ ergs s$^{-1}$ via $\nu\bar{\nu}$ annihilation in baryon-devoid regions and drives in this way a relativistic, bipolar outflow (Rosswog & Ramirez-Ruiz 2002; Aloy et al. 2005). The surrounding baryonic material collimates these jets into a small fraction of the solid angle so that they appear as isotropized, $\sim 10^{50}$ ergs (Rosswog & Ramirez-Ruiz 2003). As the neutrino annihilation rate scales roughly with the neutrino luminosity squared, the most promising cases of this study ($q = 0.1$) provide $L_{\rm jet,NSBH} \approx 3 \times 10^{48}\ [10^{51}/(2 \times 10^{53})]^2$ ergs s$^{-1}$ $\approx 10^{43}$ ergs s$^{-1}$ for about 10 ms. This estimate is rather on the optimistic side as, due to the thin-disk geometry in the NSBH case, the probability for neutrinos to collide close to head-on (where the annihilation cross section is maximal) is severely reduced. Moreover, such disks do not provide powerful winds from neutrino ablation to collimate a possible outflow. Therefore, the signal resulting from neutrino annihilation may be even less luminous. General relativistic effects such as the bending of neutrino trajectories and the redshift of the neutrino energy may influence the result, but their influence goes in opposite directions and changes the nonrelativistic results only by a factor of about 2 (Asano & Fukuyama 2001). Recently, Ramirez-Ruiz & Socrates (2005) have argued that neutrino spectra substantially different from blackbody may increase the overall explosion efficiency by more than an order of magnitude. But even if we stretch all of the available parameters to their most optimistic limits, e.g., assuming 1 order of magnitude more efficiency from neutrino spectra and an (ad hoc) extremely small beaming fraction, $\zeta = \Omega/2\pi \sim 10^{-3}$, it is hard to see how the apparent isotropized luminosity should exceed, say, $10^{47}$ ergs s$^{-1}$ (for about 10 ms) even in the most promising cases of this study.

Another agent that could possibly feed energy into collimated outflow is the magnetic field. Being naturally endowed by strong magnetic fields to start with, the shredding of a neutron star could be expected to be a good candidate for magnetic field amplification. This may occur via various pathways, the fastest of which is probably the magnetorotational instability (Velikhov 1959; Chandrasekhar 1960; Balbus & Hawley 1998 and references therein). Figure 10 shows the evolution of the disk-averaged magnetic field,

$$\langle B^{\rm eq} \rangle = \sqrt{8\pi}\frac{\sum_i m_i \sqrt{\rho_i} c_{s,i}}{\sum_i m_i}, \qquad (1)$$

making the extreme assumption that the field can reach equipartition field strength. Here the index $i$ runs over the particles

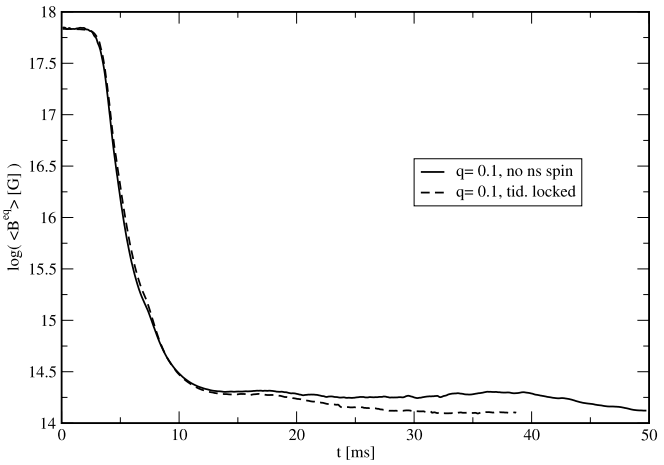


FIG. 10.—Equipartition field strengths for runs 2 ($q = 0.1$; tidal locking; *dashed line*) and 7 ($q = 0.1$; no neutron star spin; *solid line*) of the neutron star material averaged over the innermost 600 km ("disk") as a function of time.

inside 600 km (see Fig. 4) around the hole, $m_i$ are the masses, $\rho_i$ are the densities, and $c_{s,i}$ are the sound velocities of the SPH particles. Under this assumption an average field strength slightly in excess of $10^{14}$ G would result. Making the most optimistic assumptions, we estimate the properties of the possibly resulting fireball (see Piran [1999] for a fireball review). The fireball energy is $E \sim \langle B^{\rm eq}\rangle^2/8\pi V_{\rm isco} \approx 4 \times 10^{48}$ ergs $B_{14}^2(M_{\rm BH}/15\ M_\odot)^3$. This yields an initial fireball temperature of $T_0 \approx 3.3$ MeV$[E/(4 \times 10^{48}$ ergs$)]^{1/4}(M_{\rm BH}/15\ M_\odot)^{-3/4}$. The critical value $\eta_b$, where $\eta = E/M$, with $E$ and $M$ the energy and mass of the fireball, respectively, is given by Piran (1999): $\eta_b \approx 6000[E/(4 \times 10^{48}$ ergs$)]^{1/3}(M_{\rm BH}/15\ M_\odot)^{-2/3}$. Given the fact that the resulting disk is very thin and neutrino ablation is not important, we consider it plausible that the fireball is in the electron opacity–dominated range $\eta_b < \eta < \eta_{\rm pair} \approx 5 \times 10^8$ $[E/(4 \times 10^{48}$ ergs$)]^{1/2}(M_{\rm BH}/15\ M_\odot)^{-1/2}$. The fireball thus becomes transparent to photons before it reaches the matter-dominated stage. As the Lorentz factor grows, $\gamma \propto R$, and the fireball temperature drops, $T \propto 1/R$, the observed temperature, $T_{\rm obs} \propto \gamma T$, is that of the initial fireball. This yields a blackbody gamma-ray pulse with a temperature of about 3.3 MeV. Performing similar estimates for the fireball from neutrino annihilation yields a thermal pulse of about 2 MeV. *Swift* will have difficulties detecting it, but the *Gamma-Ray Large Area Space Telescope* (*GLAST*) should be able to see a pulse of several tens of ms out to a redshift of $z \sim 0.1$.

As mentioned previously, these estimates are based on the most optimistic assumptions. As the material plunges into the hole within about one orbit once it has passed $R_{\rm isco}$, any instability will have difficulties to amplify the field by large factors. The expected thermal precursor pulse may therefore be even weaker than that estimated above.

In summary, none of the investigated systems seems to be an obvious candidate for the central engine of the observed short-hard GRBs. Neutron star–black hole mergers may still be able to produce GRBs. Obviously, smaller mass black holes are more promising. Technically, however, they are much more challenging as the neutron star has a mass comparable to that of the black hole and spacetime is far from the Schwarzschild solution. Therefore, the use of neither pseudo-potentials nor simulations on a fixed background spacetime is justified; here fully relativistic three-dimensional simulations of the full merger process are required.

The spin of the black hole may provide a way to launch GRBs even from more massive black holes. If they are spinning very rapidly from the beginning and are spun up further during the merger to values close to the maximum spin parameter of $a = 1$, then both the position of the last stable orbit and the event horizon move to 1 $M_{\rm BH}$ (see Fig. 7). Therefore, much higher temperatures and densities can be reached in the inner disk regions. The fraction of viable GRB candidates among the NS-BH systems obviously depends on their mass and initial BH spin distribution. Neither quantity is observationally known, and predictions of them via population synthesis models are plagued by large uncertainties. It is clear, however, that the whole available parameter space will not provide conditions that are favorable to launch GRBs. This fact, as well as the nonobservation of even a single neutron star–black hole system (while eight double neutron star systems are observed), makes it plausible that the observed short-hard GRBs are dominated by double neutron star coalescences.

### 4.3. *Electromagnetic Transients*

In the investigated NS-BH mergers we find very large amounts of radioactive material being ejected. The radioactive decay of this debris material would, like in a Type Ia supernova, power the postcoalescence light curve. The bulk of ejecta material stems from the initial nucleon fluid of the neutron star and ends up in large, possibly *r*-process nuclei. If we assume a typical nuclear binding energy of $\sim$8 MeV per nucleon for the final nuclei, the decompression of this material releases, depending on the mass ratio of the NS-BH system, between $\sim 1.6 \times 10^{50}$ and $\sim 3.2 \times 10^{51}$ ergs from radioactive decays. The details of the resulting light curve depend on the nuclear binding energies and decay timescales and their competition with the expansion of the material. As these nuclei would be extremely neutron-rich (see Fig. 9) and far away from the valley of $\beta$-stability, no experimental data for their half-lives are available, and one would have to resort to theoretical predictions. For a simple estimate of the resulting electromagnetic transient from these radioactive ejecta, we use the simple analytical estimate of Li & Paczyński (1998), who assumed spherical symmetry and a uniform distribution of nuclear lifetimes in logarithmic time intervals. Scaling their results with the numbers found in our simulations, we find that the peak luminosity of $\sim 6 \times 10^{44}$ ergs s$^{-1}$ should be reached about 3 days after the coalescence (the "banana-like" geometry may lead to a peak that occurs somewhat later than that in the spherical model of Li & Paczyński ). The effective temperature at peak would be $\sim 10^4$ K and would result in an intensity maximum in the optical/near-infrared band of the spectrum.

It is worth pointing out, however, that this result relies on radioactive nuclei still being present when the ejecta become optically thin, which depends on the details of the nuclear reaction path. It may also be possible that the decays have ceased already by that time and that the result is essentially a "dark explosion." This interesting topic definitely deserves further examination.

In summary, the merger of a neutron star with a black hole of a mass beyond 14 $M_\odot$ may, rather than producing a gamma-ray burst, yield a supernova-like transient with a thermal precursor pulse peaking in the gamma-ray band. Such a precursor of $\sim$10 ms duration should be detectable with *GLAST* out to a redshift of $z \sim 0.1$. Follow-up observations should then be able to detect, a few days later, the supernova-like transient.

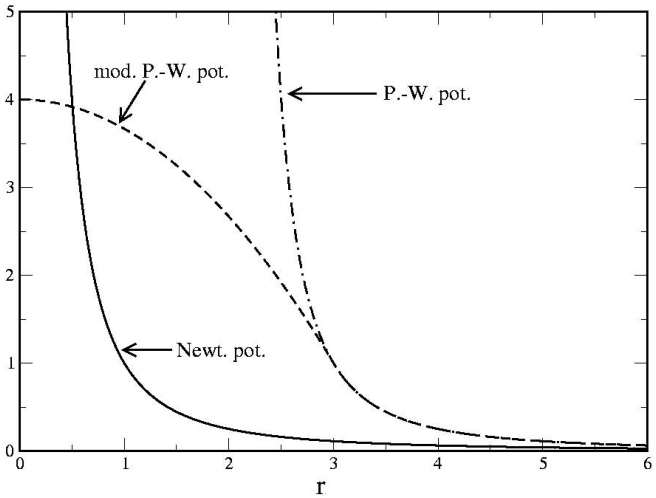


FIG. 11.—Comparison of the denominator for purely Newtonian, Paczyński-Wiita, and modified Paczyński-Wiita forces introduced to avoid the singularity at $2M_{\rm BH}$ (for a transition radius, $R_t = 3M_{\rm BH}$; see the Appendix for details). All particles that have ever been inside $R_t$ are removed.

It is a pleasure to thank Marek Abramowicz, Jim Lattimer, William Lee, Andrew MacFadyen, Enrico Ramirez-Ruiz, Roland Speith, and Christophe Winisdoerffer for useful discussions, and the INFN in Catania and the IAS in Princeton for their hospitality. The calculations reported here have been performed on the JUMP supercomputer of the Höchstleistungsrechenzentrum Jülich.

## APPENDIX

## PACZYŃSKI-WIITA POTENTIAL WITH SMOOTH EXTENSION

Here we show the form of the potential that is used in the simulations. To numerically avoid the singularity at the Schwarzschild radius, we extend the Paczyński-Wiita acceleration denominator, $D_{\rm PW} = 1/(r - R_s)^2$, smoothly down to a vanishing radius with a polynomial $D_{\rm pol}$ that possesses the following properties:

1. It matches $D_{\rm PW}$ at a transition radius, $R_t$: $D_{\rm PW}(R_t) = D_{\rm pol}(R_t)$.
2. The derivatives match smoothly: $(dD_{\rm PW}/dr)(R_t) = (dD_{\rm pol}/dr)(R_t)$.
3. Its derivative vanishes in the origin: $(dD_{\rm pol}/dr)(0) = 0$.

Using $A = R_t^{-1}(R_s - R_t)^{-3}$ and $B = (R_s - 2R_t)/(R_s - R_t)^3$, the force denominator is expressed as

$$D = \begin{cases} Ar^2 + B & \text{for } r < R_t, \\ 1/(r - R_s)^2 & \text{for } r \geq R_t. \end{cases}$$

The form of $D$ is shown in Figure 11; we always use $R_t = 3\,M_{\rm BH}$. Note that every particle that has ever been inside $R_t$ is removed at the next dump step (the time between two subsequent dumps is a small fraction [$\approx$1/12] of the neutron star dynamical time).

## REFERENCES

Abramovici, A., et al. 1992, Science, 256, 325
Abramowicz, M. A., Beloborodov, A. M., Chen, X. M., & Ihumenshchev, I. V. 1996, A&A, 313, 334
Aloy, M. A., Janka, H.-T., & Muller, E. 2005, A&A, 436, 273
Argast, D., Samland, M., Thielemann, F.-K., & Qian, Y.-Z. 2004, A&A, 416, 997
Artemova, I. V., Bjoernsson, G., & Novikov, I. D. 1996, ApJ, 461, 565
Asano, K., & Fukuyama, T. 2001, ApJ, 546, 1019
Balbus, S. A., & Hawley, J. F. 1998, Rev. Mod. Phys., 70, 1
Balsara, D. 1995, J. Comput. Phys., 121, 357
Benz, W., Bowers, R., Cameron, A., & Press, W. 1990, ApJ, 348, 647
Bethe, H. A., & Brown, G. E. 1998, ApJ, 506, 780
Bloom, J. S., et al. 2005, ApJ, in press (astro-ph/0505480)
Caron, B., et al. 1997, Classical Quantum Gravity, 14, 1461
Chandrasekhar, S. 1960, Proc. Natl. Acad. Sci., 46, 53
Eichler, D., Livio, M., Piran, T., & Schramm, D. 1989, Nature, 340, 126
Fehlberg, E. 1968, NASA Tech. Rep. TR-R-287 (Washington: GPO)
Freiburghaus, C., Rosswog, S., & Thielemann, F.-K. 1999, ApJ, 525, L121
Fryer, C. L., & Kalogera, V. 2001, ApJ, 554, 548
Gingold, R. A., & Monaghan, J. J. 1983, MNRAS, 204, 715
Goodman, J. 1986, ApJ, 308, L47
Janka, H.-T., Eberl, T., Ruffert, M., & Fryer, C. L., 1999, ApJ, 527, L39
Kouveliotou, et al. 1993, ApJ, 413, L101
Lattimer, J., & Schramm, D. N. 1974, ApJ, 192, L145
———. 1976, ApJ, 210, 549
Lee, W. H. 2000, MNRAS, 318, 606
———. 2001, MNRAS, 328, 583
Lee, W. H., & Kluzniak, W. L. 1999a, ApJ, 526, 178
———. 1999b, MNRAS, 308, 780
Lee, W. H., & Ramirez-Ruiz, E. 2002, ApJ, 577, 893
Lee, W. H., Ramirez-Ruiz, E., & Granot, J. 2005a, ApJ, 630, L165
Lee, W. H., Ramirez-Ruiz, E., & Page, D. 2004, ApJ, 608, L5
———. ApJ, 2005b, 632, 421
Li, L.-X., & Paczyński, B. 1998, ApJ, 507, L59
Mészáros, P. 2002, ARA&A, 40, 137
Miller, M. C. 2005, ApJ, 626, L41
Morris, J., & Monaghan, J. 1997, J. Comp. Phys., 136, 41
Novikov, I. D., & Frolov, V. P. 1989, Physics of Black Holes (Dordrecht: Kluwer)
Paczyński, B. 1986, ApJ, 308, L43
———. 1991, Acta Astron., 41, 257
Perna, R., & Belczynski, K. 2002, ApJ, 570, 252

Pfahl, E., Podsiadlowski, P., & Rappaport, S. 2005, ApJ, 628, 343
Piran, T. 1999, Phys. Rep., 314, 575
———. 2005, Rev. Mod. Phys., 76, 1143
Ramirez-Ruiz, E., & Socrates, A. 2005, ApJ, submitted (astro-ph/0504257)
Rasio, F., Faber, J., Kobayashi, S., & Laguna, P. 2005, preprint (astro-ph/0503007)
Rosswog, S., & Davies, M.-B. 2002, MNRAS, 334, 481
Rosswog, S., Davies, M. B., Thielemann, F.-K., & Piran, T. 2000, A&A, 360, 171
Rosswog, S., & Liebendörfer, M. 2003, MNRAS, 342, 673
Rosswog, S., & Ramirez-Ruiz, E. 2002, MNRAS, 336, L7
———. 2003, MNRAS, 343, L36
Rosswog, S., Ramirez-Ruiz, E., & Davies, M. B. 2003, MNRAS, 345, 1077
Rosswog, S., Speith, R., & Wynn, G. A. 2004, MNRAS, 351, 1121
Setiawan, S., Ruffert, M., & Janka, H.-T. 2004, MNRAS, 352, 753
Shen, H., Toki, H., Oyamatsu, K., & Sumiyoshi, K. 1998a, Nucl. Phys. A, 637, 435
———. 1998b, Prog. Theor. Phys., 100, 1013
Stairs, I. H. 2004, Science, 304, 547
Tagoshi, H., et al. 2001, Phys. Rev. D, 63, 062001
Taniguchi, K., Baumgarte, T. W., Faber, J. A., & Shapiro, S. L. 2005, Phys. Rev. D, 72, 044008
Velikhov, E. P. 1959, Sov. Phys.– JETP Lett., 36, 995
Wiilke, B., et al. 2003, Proc. SPIE, 4856, 238